Monte Carlo simulations of surface reactions

ELSEVIER

Applied Catalysis A: General 160 (1997) 99–123

APPLIED CATALYSIS A: GENERAL

Monte Carlo simulations of surface reactions

R.M. Nieminen, A.P.J. Jansen*

Laboratory of Physics, Helsinki University of Technology, FIN-02150 Espoo, Finland

Abstract

Numerical simulations based on the Monte Carlo method offer a powerful approach for detailed studies of complex reaction sequences, such as those associated with heterogeneous catalysis. In this article, we summarize some of the recent work based on discrete models for irreversible surface reactions. Particular emphasis is placed on kinetic phase transitions, bistability, and oscillatory (nonstationary) reactions. In addition to discussing some of the fundamental aspects of nonequilibrium kinetics, we show through specific examples that explicit Monte Carlo simulations can transcend traditional approaches based on rate-equation methods, in particular those invoking the mean-field approximation. This is particularly the case when local correlations and fluctuations among the reactants are important.

Keywords: Monte Carlo simulation; Surface reaction; Kinetics

1. Introduction

From the point of view of statistical physics, heterogeneous catalysis under typical flow conditions is a prime example of a system whose macroscopic steady state is not described by thermal equilibrium [1]. The reactive steady state is characterized by macroscopic averages slowly varying in time, and yet the probability of observing a given microscopic state of the system is not determined by the Boltzmann distribution.

There is considerable current interest in understanding the behavior of such systems, which in fact are quite common in nature. Such systems are usually open and subject to external driving forces. Examples of physical systems in this class include Rayleigh–Benard convection [2], nonlinear optical materials [3], biological models for the spreading of diseases and bacterial colonia [4], self-organized criticality [5], traffic flow models [6], spinodal decomposition [7], etc.

Among the generic features of such nonequilibrium steady-state systems is that they can undergo a 'phase transition', meaning that the macroscopic variables (such as the yield of a chemical reaction) may undergo a singular change when the rates of the various microscopic processes are smoothly changed. A first-order transition signifies a jump, for example, in the coverage of a reactant on the catalyst surface. A higher-order transition implies a continuous change in the coverage but singularities in higher-order correlation functions, e.g. the mean-square density. However, unlike in systems in thermal equilibrium one cannot relate these quantities to derivatives of the free energy.

The absence of thermodynamic equilibrium in such systems means that it is possible to find steady states

*Corresponding author. Permanent address: Laboratory of Inorganic Chemistry and Catalysis, Eindhoven University of Technology, 5600 MB Eindhoven, Netherlands.

PII S0926-860X(97)00130-0

varying on several length or time scales. The spatio-temporal behavior can be periodic, quasiperiodic, or even chaotic. The steady state may thus exhibit spatial modulations, possibly coupled to temporal waves to produce reaction waves and fronts. For example, there is an extensive literature on catalytic surface reactions with temporal and spatial oscillations, including CO oxidation on Pt-group metals [8–10], NO–CO reactions on Pt and Pd [11–13], and oxidation of H_2 on Pt [14,15].

The straightforward method to characterize and model nonequilibrium systems is to define a set of rules with associated probabilities for how the system evolves in its phase space from one configuration to another, and then describe the system in terms of so-called rate equations. For heterogeneous catalysis the phase space is spanned by the positions that can be occupied by the various chemical species present in the reaction system. The rules and probabilities would model the various reaction steps: adsorption, dissociation, surface diffusion, reactions, desorption of reaction products, etc. Such dynamical rules can incorporate the knowledge of the individual reaction steps and substrate properties obtained from several surface science studies.

The dynamical behavior of the system can then be formulated in terms of a Master Equation for the rate of change of the probabilities of observing each microstate. The Master Equation depends on parameters (rate constants) that can be derived from microscopic rules and probabilities; they replace such intensive variables as temperature and chemical potential familiar from equilibrium systems. Since the microscopic rates usually do not obey detailed balance in nonequilibrium systems, one cannot in general determine the steady-state probability distributions.

A popular simplification to be invoked for such systems and the relevant rate equations is the mean-field approximation, where one replaces the time-varying quantities by their temporal averages and/or spatially fluctuating quantities by their mean values [16]. Such mean-field models then lead to kinetic equations, which, even though usually nonlinear and coupled, are at least amenable to numerical solutions; often even analytical solution is possible. However, it is clear that such models may miss some or all of the more intricate properties of the nonequilibrium steady-state system. Moreover, such sets of stiff differential equations can have serious nonphysical instabilities.

For surface processes such as heterogeneous catalysis, the mean-field approach usually invokes Langmuir's adsorption model and rate equations based on the law of mass action [17,18]. These are written in terms of (partial) differential equations involving the reactant concentrations on the surface and in the gas phase. They may also invoke the convection due to concentration and thermal gradients. The time evolution of the set of equations is then studied as the rate coefficients are varied. Of particular fundamental interest are then the unusual solutions such as oscillatory and chaotic behavior that the solutions may show.

Mean-field theory implicitly assumes that coarse-grained averages, say, for surface concentrations, can be obtained accurately from averaged rate equations that ignore any local correlations. However, in surface catalysis it is obvious that local correlations can be important. The reactions can only take place between surface atoms or molecules in contact. Likewise, surface impurities can block sites, inhibit reactivity in their vicinity (poisoning) or locally increase the reaction rate (promotion). Reactants can be spatially segregated under the influence of high reaction rates so that the relevant reaction speed has little to do with the macroscopically averaged concentrations.

By now there is substantial evidence for the 'anomalous kinetics' [19] arising from the important role of local correlations and fluctuations. Further complexity is added by the existence of precursor states and lateral interactions, both adding to the complexity of the kinetics of surface rate processes [20]. It then becomes necessary to go beyond the mean-field type approaches for a proper understanding of the system, including its steady-state behavior and possible phase transitions.

In this article, we summarize some of the recent work on nonequilibrium kinetics of heterogeneous catalysis. Rather than covering the vast literature on rate equation modeling, we mainly focus on direct Monte-Carlo-type simulations of surface reactions. The Monte Carlo method is vastly popular in equilibrium statistical physics [21], where the Boltzmannian phase space density can be effectively sampled through the Metropolis algorithm. The

method can readily be generalized to the nonequilibrium case.

Through comparison with rate equation approaches, we point out some of the unexpected and nontrivial generic features of selected model systems to underline the importance of local correlations in producing interesting temporal and spatial behavior. These features elucidate such effects as bistability between poisoning and reactivity, the associated critical properties, effects of diffusion, desorption and lateral interactions, effects of substrate instabilities, and mechanisms for oscillatory behavior. We will not attempt at a comprehensive review, but rather focus on a few examples, taken mainly from our own published work.

The basic ideas of Monte Carlo simulation of relevant lattice models are summarized in Section 2, where particular emphasis is placed on the interpretation of time scales in dynamical simulations. Two classes of model systems are discussed in Section 3. The first class includes the Ziff–Gulari–Barshad (ZGB) model for dimer–monomer reactions with its several extensions [22]. The ZGB-models are simple yet nontrivial descriptions of catalytic surface reactions, and isolate the salient features of large classes of reaction systems. The second class of model systems discussed in Section 3 is built around the Lotka model, which enables one to critically evaluate approximate theories of chemical kinetics [23]. Here the temporal behavior of reaction system is of particular interest.

In addition to outlining some of the fundamental questions we also demonstrate the utility of Monte Carlo simulations as a practical tool for modeling and analyzing complex reaction systems. Monte Carlo simulation schemes are in general straightforward to implement, and they offer a powerful alternative to kinetic equation modeling. It will be emphasized that the local surface geometries and boundary conditions can be adopted in a straightforward manner through discrete lattice-gas-type models. Complicated reaction sequences are conceptually easily handled in terms of the local rules and associated probabilities. Lateral interactions between adatoms can be incorporated in a transparent way.

We discuss two explicit examples in Section 4. The first is the modeling of temperature-programmed desorption (TPD) [24,25]. Special attention is paid to temporal behavior and lateral interactions. As the second example, we discuss in some detail the modeling of CO hydrogenation on model catalysts [26]. Building alternative models for the fairly complicated reaction sequence and comparing against experimental yield curves makes it possible to identify the important mechanisms and the bottlenecks controlling the overall efficiency and product distributions.

2. Monte Carlo simulation methods

Various stochastic (Monte Carlo) simulation methods can be used to investigate surface reactions. Most of the techniques utilize the lattice-gas model, where the surface region is described by a discrete, regular two- or three-dimensional array of lattice sites. The reactant atoms and molecules occupy the sites, and are added to the system from a reservoir of the gas phase. The atoms and molecules adsorb, dissociate, diffuse, react and desorb according to the corresponding probabilities and rules. Mathematically, each grid point has a label that stands for the occupation of the corresponding site. The occupation numbers are successively updated according to the reaction rules and rates. The system evolves dynamically, and may or may not eventually reach a quasi-equilibrium steady state. The updating can take place sequentially in various ways, or in parallel as in a cellular automaton. We outline here the most frequently used updating methods and comment on their interpretation.

The simplest method is as follows. First a lattice site is chosen randomly. All possible reaction steps are checked to see which ones are possible at that site. The reactions may, of course, involve neighboring sites. The occupation numbers are then changed according to the possible reactions with probabilities that reflect the rate constants.

Then the next site is chosen. After each site has been visited on an average once, a Monte Carlo time step has been completed. The full simulation consists of a large number of such steps. The total physical time is expressed in the number of Monte Carlo steps.

This method is popular in particular for cases where one is interested in reaction systems under steady-state conditions. Then in fact the actual route how the quasi-equilibrium has been reached does not matter. Examples of Monte Carlo simulations using this method are given in Section 4.

For systems that do vary in time, it is not clear how to determine uniquely the probabilities with which one chooses the reaction steps. Fichthorn and Weinberg [27] have discussed the dynamical interpretation of standard Monte Carlo methods used to obtain statistical averages. They have derived conditions under which the evolution of the system during a Monte Carlo simulation corresponds to real-time evolution. Let each possible reaction step i have a rate constant k_i. If there are N_i reactions of type i that can occur independently, then a time lapse

$$\Delta t = -\frac{\ln r}{\Sigma_j N_j k_j} \tag{1}$$

is generated, where r is a uniform random deviate with $0<r<1$. The following steps are then repeated: (1) time is increased by Δt; (2) the system is changed with reaction i occurring with the probability $N_i k_i / \Sigma_j N_j k_j$; (3) after the reaction step has been completed the numbers N_i are updated. Sometimes the determination of Δt is simplified by using the average step size

$$\Delta t = \frac{1}{\Sigma_j N_j k_j}. \tag{2}$$

It is not clear how important the errors that this approximation introduces are.

The method of Fichthorn and Weinberg can be justified for systems in equilibrium. It is often assumed that it is also correct for nonequilibrium cases. The method does not explicitly specify how to obtain the rate constants k_i. Meng and Weinberg [28] have extended the method to simulate TPD experiments, a topic discussed at greater length in Section 4. They assume that the rate constants change only negligibly in the interval Δt and that values (at the temperature) of the starting instant of Δt can be used. It is clear, however, that the rate constants do change with time. Consequently $\Delta t = 1/\Sigma_j N_j k_j$ will be systematically too large. This is particularly the case in the beginning of the simulation when the rate constants are small.

The temporal evolution of lattice-gas models is quite generally described by the Master Equation [25]:

$$\frac{\mathrm{d}P_{\{s_i\}}}{\mathrm{d}t} = \left[W_{\{s_i\}\{s_{i'}\}} P_{\{s_{i'}\}} - W_{\{s_{i'}\}\{s_i\}} P_{\{s_i\}}\right] \tag{3}$$

in statistical physics literature. Here s_i stands for the occupation of site i, $\{s_i\}$ denotes the occupations of all sites, i.e the configuration of the system. $P_{\{s_i\}}$ is the probability to find the system in configuration $\{s_i\}$, and $W_{\{s_i'\}\{s_i\}}$ is the transition probability per unit time for the process that changes the system from configuration $\{s_i\}$ to configuration $\{s_i'\}$. The transition probabilities are the microscopic analogs of rate constants. It is important that this equation describes the evolution in real time, and it should not be confused with the Master Equation of the dynamical interpretation of standard Monte Carlo methods. In fact, the above equation can be derived from first principles. In thermal equilibrium, the derivation yields expression for the transition probabilities of the familiar form

$$W_{\{s_i'\}\{s_i\}} = \exp\left[-\frac{\Delta E_{\mathrm{act}}}{RT}\right], \tag{4}$$

where ΔE_{act} denotes the activation free energy for the microscopic reaction step in question. This means that the transition probabilities can be determined in principle using quantum chemical methods.

There are a number of methods for approximate solving of the Master Equation, and for some systems it is even possible to solve it exactly. Here we are naturally interested in solving it using stochastic (Monte Carlo) methods. If the transition probabilities are time-independent, one method is equivalent to that of Fichthorn and Weinberg [27,29,30]. We have

$$\Delta t = -\frac{\ln r}{\Sigma_{\{s_i'\}} W_{\{s_i'\}\{s_i\}}}, \tag{5}$$

and the reaction that changes $\{s_i\}$ to $\{s_i'\}$ should be chosen with the probability $W_{\{s_i'\}\{s_i\}} / \sum_{\{s_i''\}} W_{\{s_i''\}\{s_i\}}$. Alternatively it is possible to determine a time step $\Delta t_{\{s_i'\}\{s_i\}}$ for each reaction [25] as

$$\Delta t_{\{s_i'\}\{s_i\}} = -\frac{\ln r}{W_{\{s_i'\}\{s_i\}}}. \tag{6}$$

The reaction that occurs first is the one with the smallest time step. This method is somewhat less efficient than the previous one, but has the advantage that in can be extended to situations where the transition probabilities are explicitly time-dependent. For example, in TPD simulations with linear time dependence for temperature analytical expressions can be derived for $\Delta t_{\{s_i'\}\{s_i\}}$ (see Section 4 below).

3. Simple systems

There is no fundamental difference between the systems of this section and those of the next. Yet there are good reasons to treat them separately. We call the systems of this section 'simple', because it is possible to obtain highly accurate numerical results by using Monte Carlo simulations, while one can also apply many approximate theories and test them in detail.

There need be nothing simple about the behavior of simple systems. They show kinetic phase transitions, bifurcations, oscillations, chaos, etc. In fact, they are often also used to isolate some specific behavior and to determine the mechanisms that causes it. This knowledge can then be used to interpret the behavior of more complex systems.

The systems that are treated in this section are not the simplest one can imagine. Unimolecular reactions, like monatomic desorption and adsorption, can often be treated exactly using simple analytical methods [25,31]. Exact results can also be obtained for some bimolecular reactions, e.g., 1D models of annihilation and coagulation [32]. Here we will discuss the Ziff–Gulari–Barshad model and the Lotka model. For these systems there are few analytical results, and Monte Carlo simulations have to be used to obtain results that are numerically exact. One should also emphasize that the focus in this section is in discussing the nontrivial generic features of such models rather than in modeling specific surface reactions in detail.

3.1. The Ziff–Gulari–Barshad model and some extensions

The Ziff–Gulari–Barshad model (ZGB-model) describes the oxidation of CO on a catalytic surface. In its original form it contains only three reactions [22]:

$$\mathrm{CO(gas)} + * \rightarrow \mathrm{CO(ads)}, \tag{7}$$

$$\mathrm{O_2(gas)} + 2* \rightarrow 2\mathrm{O(ads)}, \tag{8}$$

$$\mathrm{CO(ads)} + \mathrm{O(ads)} \rightarrow \mathrm{CO_2} + 2*. \tag{9}$$

Here $*$ represents a vacant site, and the two sites involved in the last two reactions are nearest neighbors. The sites are assumed to form a regular lattice, for example a square grid. The formation of CO_2 is assumed to occur immediately after a CO and an oxygen atom become adsorbed on neighboring sites. The adsorption of CO and O_2 can have a finite rate constant.

Fig. 1 shows the main result of Monte Carlo simulations of the ZGB-model [22]. The CO_2 production is clearly not a simple function of the rate constants; there is even a discontinuity. The parameter y is defined as the fraction of all molecules in the gas phase that are CO molecules, and we assume that sticking coefficients are equal to unity. We can distinguish three ranges. If $y<y_1\approx 0.3873\pm 0.0001$ [33] the CO pressure is low compared to the O_2 pressure. As a consequence the surface is completely covered by oxygen, and no CO_2 is produced. For $y_1<y<y_2=0.52560\pm 0.00001$ [34] the CO adsorption is competitive with oxygen adsorption, and the CO_2 production increases with CO pressure. The transition at y_1 is a second-order (continuous) kinetic phase transition. For $y>y_2$ the O_2 pressure is low compared to the CO pressure, we have CO poisoning, and again no CO_2 is produced. The kinetic phase transition at y_2 is first order, because the CO_2 production rate changes discontinuously. Once the reaction conditions have been defined by fixing the single parameter y, the phase diagram is uniquely defined.

In the original ZGB-model the poisoned states remain stable once they have formed, as there is no reaction to remove adsorbates after the surface has become completely covered by either CO or oxygen, i.e. no desorption. Thus by sweeping the reaction conditions the system can find itself in the 'wrong' state, i.e. exhibit bistable or hysteretic behavior. As will be shown below, this so-called multiplicity plays a role in some mechanisms that cause oscillations.

Before describing extensions of the original ZGB-model, we would like to present the results one obtains by applying macroscopic rate equations [35]. In the mean-field approximation, the rate equations for the CO and O coverages are given by

$$\frac{\mathrm{d}\theta_{\mathrm{CO}}}{\mathrm{d}t} = y\theta_* - 4K\theta_{\mathrm{CO}}\theta_{\mathrm{O}}, \tag{10}$$

$$\frac{\mathrm{d}\theta_{\mathrm{O}}}{\mathrm{d}t} = 2(1-y)\theta_*^2 - 4K\theta_{\mathrm{CO}}\theta_{\mathrm{O}}, \tag{11}$$

where K is the rate constant for the oxidation step ($K\rightarrow\infty$), and the coefficient 4 is for a square grid. Time has been scaled to simplify the coefficients of the adsorption terms. Although the form of these equa-

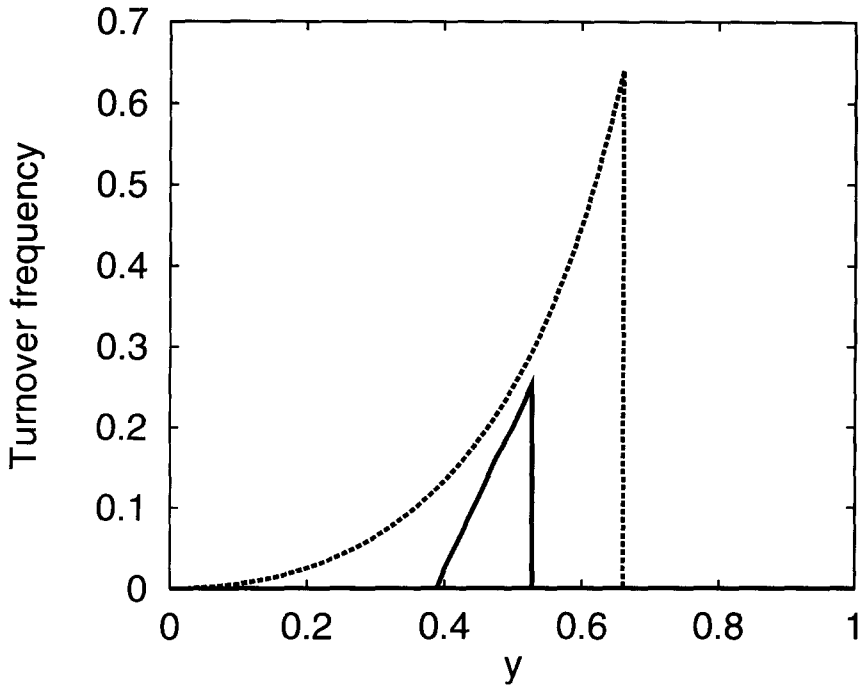

Fig. 1. The CO_2 production in the ZGB-model as a function of the CO fraction y according to the Monte Carlo simulations (solid line), and according to the macroscopic rate equations (dashed line).

tions is obvious, a comparison with the Monte Carlo results is only possible when the coefficients of the coverages on the right-hand-side are expressed in terms of the same parameters that are used in Monte Carlo. This can be done if one bases the Monte Carlo simulations on a real-time Master Equation, and derives the rate equations from this [25,36]. One needs to introduce, however, the approximation that the adsorbates are randomly distributed. For the comparison of steady-state values, temporal scaling is obviously not important.

Fig. 1 also shows the CO_2 production as a function of y from the macroscopic mean-field rate equations. The equations have two or four equilibrium points, where the time derivative of the coverages vanish. The CO-poisoned state and the O-poisoned state correspond to equilibrium points for any y. For $y < y_2' = 2/3$ there are also two reactive states (i.e. CO_2 producing states). However, the O-poisoned state is unstable, as is one of the reactive states. At y_2' there is a saddle–node bifurcation at which the reactive states annihilate and the system moves to the CO-poisoned state [37,38].

There are two obvious discrepancies between the macroscopic rate equations and the Monte Carlo results. There is a O-poisoned state in Monte Carlo, and the values of y_2 and y_2' differ substantially. The range in which there is a stable reactive state is grossly overestimated by the mean-field rate equations. Visualization of the reactive state in Monte Carlo reveals the origin of the discrepancies. The adsorbates are not randomly distributed, but form well-separated CO and oxygen islands. This allows for nonzero coverages of CO and oxygen in the reactive state, whereas the macroscopic rate equations predict that $\theta_{CO}=0$ or $\theta_O=0$ always, because $K\rightarrow\infty$ (note that $K\theta_{CO}$, respectively, $K\theta_O$ need not be zero).

Although the macroscopic rate equations written in the mean-field form have serious defects, they are computationally much less time consuming than the Monte Carlo simulations. Therefore, it is tempting to seek ways to go beyond the mean-field approximation (while retaining the computational efficiency) by

including correlations in the occupation of the surface sites [39,40]. Instead of Eqs. (10) and (11) one then has

$$\frac{d\theta_{CO}}{dt} = y\theta_* - 4K\langle \mathrm{CO\ O}\rangle, \tag{12}$$

$$\frac{d\theta_O}{dt} = 2(1-y)\langle **\rangle - 4K\langle \mathrm{CO\ O}\rangle, \tag{13}$$

where $\langle$CO O$\rangle$ is the probability that at an arbitrary horizontal pair of neighboring sites the left site is occupied by CO and the right by O, and $\langle **\rangle$ is the probability that both are vacant. These and similar quantities are called two-point probabilities (in general N-point probabilities) [39], or distributions [40]. Assuming that only nearest-neighbor reactions take place (as in the original ZGB-model), Eqs. (12) and (13) are exact. One can introduce higher-order distributions (defined in an obvious way) to write down hierarchical equations for the occupation probabilities. For example,

$$\begin{aligned}\frac{d\langle \mathrm{CO\ O}\rangle}{dt} = {} & y\langle *\mathrm{O}\rangle + \frac{1}{2}(1-y)\left[\langle \mathrm{CO}\ **\rangle + \left\langle \begin{matrix} * & \\ \mathrm{CO} & * \end{matrix}\right\rangle\right] \\ & - K\langle \mathrm{CO\ O}\rangle - K\left[\langle \mathrm{O\ CO\ O}\rangle + \left\langle \begin{matrix} & \mathrm{O} \\ \mathrm{O} & \mathrm{CO} \end{matrix}\right\rangle\right] \\ & - K\left[\langle \mathrm{CO\ O\ CO}\rangle + \left\langle \begin{matrix} & \mathrm{CO} \\ \mathrm{CO} & \mathrm{O} \end{matrix}\right\rangle\right].\end{aligned} \tag{14}$$

These equations, which depend on three-point distributions, are exact as well. However, we see the problem with this approach. We have to introduce distributions depending on the occupation of more and more sites. In fact, we get an infinite hierarchy of rate equations [39], which must be terminated by expressing an N-site distribution in terms of lower-order ones.

The mean-field approximation is the simplest such termination. It expresses all distributions as products of coverages; in particular, $\langle$CO O$\rangle = \theta_{CO}\theta_O$ and $\langle **\rangle = \theta_*^2$. This leads to the macroscopic rate Eqs. (10) and (11) we have seen before.

Approximations that use distributions of two sites or more are called cluster approximations. Well-known from the Ising model [41,42] is the Kirkwood approximation [43], based on the idea of approximating a three-point distribution as product of two-point ones. It is given by

$$\langle \mathrm{XYZ}\rangle = \frac{\langle \mathrm{XY}\rangle\langle \mathrm{YZ}\rangle\langle \mathrm{X.Z}\rangle}{\theta_X\theta_Y\theta_Z}, \tag{15}$$

where the dot in the last distribution means that the central site can be occupied by anything. This approximation has the drawback that it violates sum rules like

$$\sum_Z \langle \mathrm{XYZ}\rangle = \langle \mathrm{XY}\rangle. \tag{16}$$

It is, therefore, sometimes better to use another product approximation [23,44]

$$\langle \mathrm{XYZ}\rangle = \frac{\langle \mathrm{XY}\rangle\langle \mathrm{YZ}\rangle}{\theta_Y}. \tag{17}$$

This approximation fulfills at least the sum rules with summation over X and Z. This is appropriate for clusters where X and Z are not neighbors, but not for the triangular clusters that one has on hexagonal grids. Mai et al. have applied the cluster approximation to the ZGB-model, and have found a clear improvement with respect to the mean-field approximation [40].

Apart from the fact that one expects cluster approximations to be more accurate than the mean-field approximation there are some other aspects that deserve attention. There is, of course, the practical problem that, as the number of differential equations increases, it becomes harder to determine the steady states. More important is that qualitatively different behavior may be obtained. If we use only equations for θ_{CO} and θ_O, i.e., only two differential equations, as in the mean-field theory, it can be shown that the steady state can only be an equilibrium point or a limit cycle [37]. For Eqs. (10) and (11) it has even been shown that the steady state is an equilibrium point, which means that there can be no oscillations in the context of mean-field theory [45]. With more than two differential equations, i.e. beyond mean-field theory, much more complex behavior, including chaotic, becomes possible. We would like to point to what seems to be a very fundamental problem with these equations, however. Oscillations and chaotic behavior are a consequence of nonlinearity. In the hierarchy of exact equations nonlinearity is hidden in the higher-order terms. Thus the approximation used to truncate the hierarchy affects the consequences of the nonlinearity,

and the results depend even qualitatively on the approximation used. This makes the specific interpretations of nonlinearity somewhat suspect.

There exist various extensions of the original ZGB-model, most of which have been added to make it more realistic in describing catalytic surface reactions. Processes that have been added include desorption of CO and O_2 [40,46–58], diffusion of the adsorbates [45–47,52,59–63], an Eley–Rideal mechanism for the oxidation step [51,64], and physisorption of the reactants [50,64,65]. The reactions have been modified to include lateral effects [46,66–68], and the rate constant of the oxidation step has been made finite [46,47,56,57,63,69]. The surface has been modified by blocking sites to model poisoning by lead [70] or alloying [71]. In order to obtain oscillations the oxygen adsorption has been made dependent on the CO coverage [72]. The reconstruction of the surface has been added [73] and an inert adsorbate has been introduced [36]. We will make a few remarks about some of these extensions, and then take a closer look at the effect of an inert adsorbate.

The diffusion of the adsorbates is interesting, because it has implications for our evaluation of the approximations that we have discussed before. One would expect that if the diffusion is much faster than the other reactions that the adsorbates will be distributed homogeneously over the surface, and that the mean-field approximation will give accurate results. According to some authors this is indeed the case [47,61]. However, there are indications that even in the limit of infinitely fast diffusion the mean-field approach is not quantitatively correct [32]. Monte Carlo results show that the first-order transition should shift to higher values of y and the second-order transition to lower values of y when diffusion is included. Within the mean-field theory, the first-order transition seems to shift only to about $y=0.5951\pm0.0002$ and $y=2/3$ is only a spinodal point [62]. The reason for the difference is that mean-field theory neglects fluctuations as well as local correlations.

The most important effect of desorption is that it allows the system to get out off the states where the surface is poisoned by CO or oxygen. It does this by creating vacancies where the other adsorbate can adsorb. This is important for the existence of oscillations as will be shown below. Another effect is that the reactive state is stable at higher values of y. If the rate constant for desorption is above some critical value, the first-order transition becomes second order [55].

If an inert adsorbate is included that only adsorbs and desorbs, but does not participate in the oxidation, then it is possible that the system oscillates [36]. This can be seen in Fig. 2. The explanation for this effect is as follows. The rate constants for CO and O_2 adsorption should be such that only the reactive state is stable when there is no inert adsorbate on the surface. If we increase the coverage θ_X of the inert adsorbate the adsorption is suppressed. As O_2 needs two sites its adsorption is reduced most, which destabilizes the reactive state. Hence there will be a transition to the CO-poisoned state at a certain coverage of the inert adsorbate. CO desorption must thus be included to avoid the surface becoming completely covered by CO. Starting from the CO-poisoned state and reducing θ_X by the desorption of X will lead to a transition back to the reactive state at some other value of θ_X. Fig. 3 shows the hysteresis curve that can result. If the adsorption and desorption of the inert adsorbate is slow, the oxidation will always be in a quasi-steady state. It is possible, however, that there is no stable steady state for the whole process. As a consequence, the attempt of the system to reach a steady state for θ_X leads to oscillations (see Fig. 3).

It is very interesting to visualize the adlayer at different points of the oscillatory cycle. Some snapshots are shown in Fig. 4. When the system is in the reactive state there are CO and oxygen islands. The CO islands are small. They have to grow to make the transition to the CO-poisoned state possible, which they do by configuring themselves in such a way that the inert adsorbate forms a carapace that shields them from oxygen. The transition from the CO-poisoned to the reactive state occurs when a small hole is formed via CO desorption in the CO layer, where oxygen can then adsorb. The hole is enlarged very rapidly, and a reaction front moves over the whole surface. This fast process forms the synchronization mechanism that makes the oscillations global.

3.2. *The Lotka model*

As has been mentioned before, simple systems can be used to study the essential properties of a real system by isolating them, or to study approximate

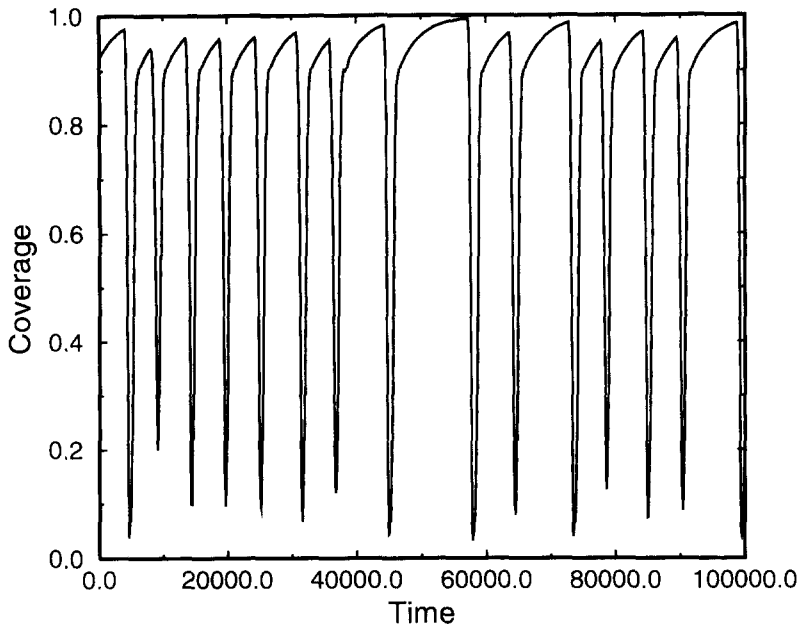

Fig. 2. The CO surface coverage as a function of time in a generalized ZGB-type model. The data has been obtained from a Monte Carlo simulation for a model where CO desorption is included, and where slow adsorption and desorption of an inert adsorbate is allowed for. The simulation grid is a 256×256 square with periodic boundary conditions. For more details, see Ref. [36].

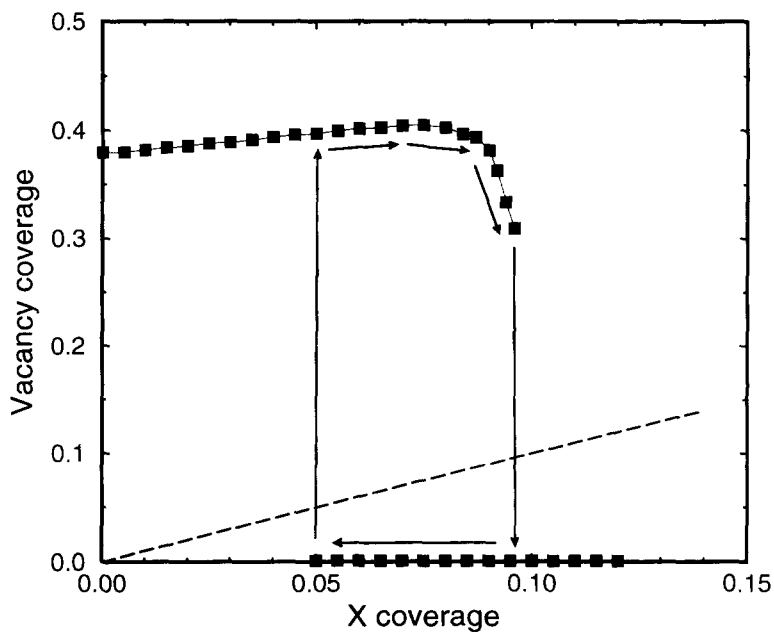

Fig. 3. The fraction of vacant sites as a function of the coverage of the inert adsorbate in a ZGB-type model with desorption of CO and with slow adsorption and desorption of an inert adsorbate X. The dashed line shows the steady-state condition for the inert adsorbate. The arrows depict the evolution of the system, determined by Monte Carlo simulation. From Ref. [36].

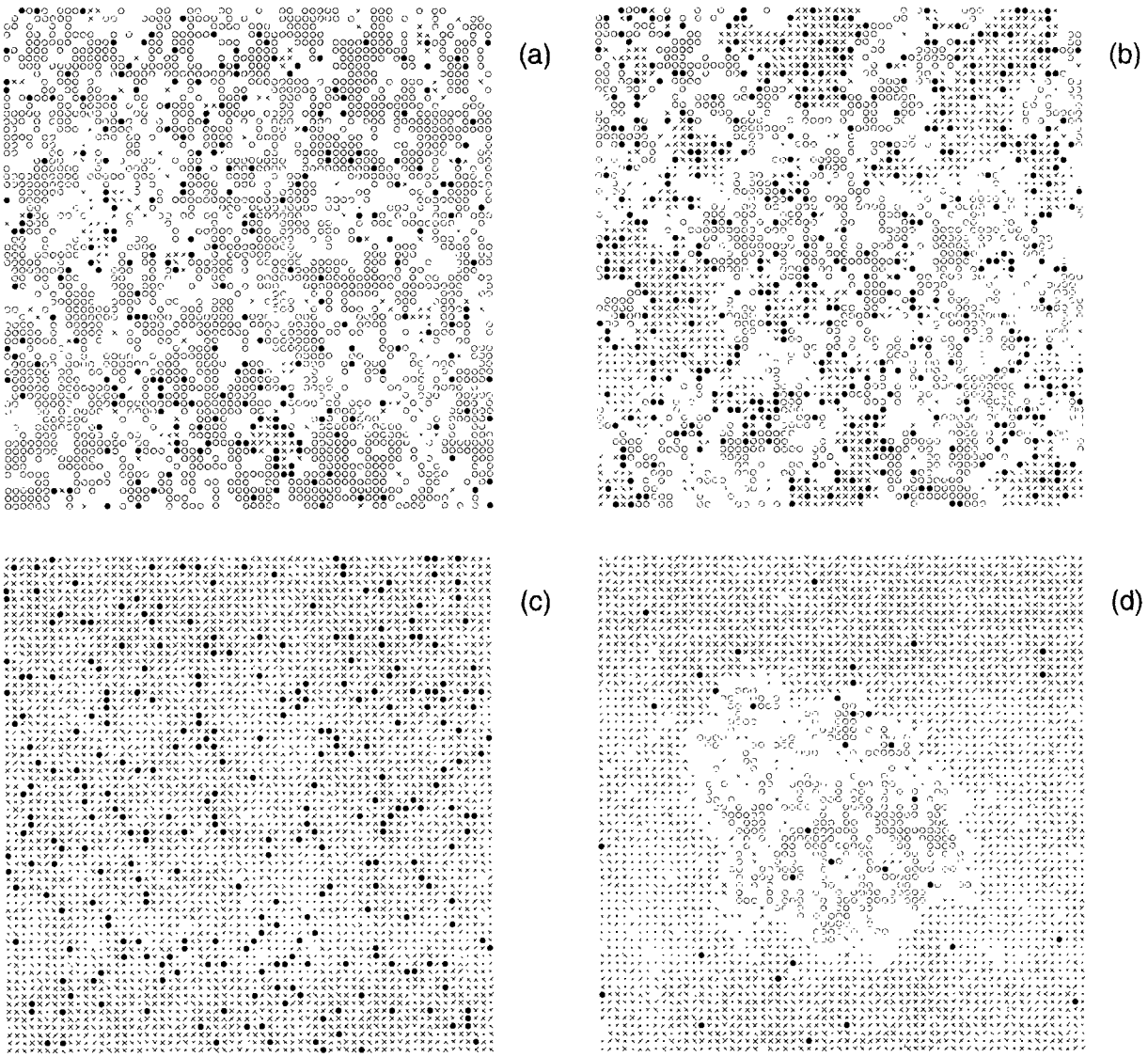

Fig. 4. Snapshots of the adlayer at different moments during one cycle of oscillation, obtained from a Monte Carlo simulation with a 64×64 square grid. The CO molecules are depicted by crosses and O atoms by open circles. The closed circles depict the inert adsorbate X. The reactive state is shown in (a), and the CO-poisoned state in (c). The transition from the reactive to the CO-poisoned state is shown in (b), and the backward transition in (d). For details of the transition probabilities in the Monte Carlo simulation, see Ref. [36].

theories of chemical kinetics. The ZGB-model is mainly an example of the former kind, whereas the Lotka model is more an example of the latter. It too consists of just three reactions [23,74]:

$$\mathrm{A(gas)} + * \rightarrow \mathrm{A(ads)}, \tag{18}$$

$$\mathrm{B(ads)} \rightarrow \mathrm{B(gas)} + *, \tag{19}$$

$$\mathrm{A(ads)} + \mathrm{B(ads)} \rightarrow 2\mathrm{B(ads)}. \tag{20}$$

In the last autocatalytic step A and B have to be nearest neighbors, and the step is infinitely fast. It is convenient to scale time so that the rate constant of the A adsorption equals ζ and that of the B desorption $1-\zeta$ with $0 \leq \zeta \leq 1$, so that the whole process is a function of just one parameter. We will mainly present results for

two-dimensional square grids, but some results for a one-dimensional and a three-dimensional cubic grid will be presented as well [74].

This system has been studied first by Mai et al. [23]. They concluded that the mean-field approximation to the rate equations gives incorrect values for the coverages of A and B, and that it even fails to predict the behavior of the model qualitatively; the Monte Carlo simulations show oscillations, whereas mean-field predicts a stable equilibrium point and a saddle point. Better values are obtained for the coverages within a cluster approximation, but also that approximation does not predict oscillations. It is thus instructive to study the oscillations more closely.

The mean-field approximation to the rate equations describing the Lotka model reads

$$\frac{d\theta_A}{dt} = \zeta\theta_* - 4K\theta_A\theta_B, \tag{21}$$

$$\frac{d\theta_B}{dt} = -(1-\zeta)\theta_B + 4K\theta_A\theta_B. \tag{22}$$

For the rate constant of the autocatalytic step $K\rightarrow\infty$ holds. The equations above are written for a square grid, which explains the coefficient 4 [25,36]. The equilibrium points of these equations are $\theta_A=1$, $\theta_B=0$, and $\theta_A=\zeta/4K$, $\theta_B=(4K-\zeta)/4K$. The A poisoned state corresponds to the saddle point, so that the system will evolve to $\theta_A=0$, $\zeta_B=\zeta$ in the limit $K\rightarrow\infty$. Fig. 5 compares this result with the Monte Carlo results. We see that especially the value for θ_A is completely incorrectly given by the mean-field approximation. The reason for this we have already seen in the ZGB-model. The fast autocatalytic step causes one of the coverages to be zero in the mean-field theory, whereas in the simulation isolated A and B islands can be formed.

The same figure shows also the results of a cluster approximation. The rate equations for the coverages and the two-site distributions are given by

$$\frac{d\theta_A}{dt} = \zeta\theta_* - 4K\langle AB\rangle, \tag{23}$$

$$\frac{d\theta_B}{dt} = -(1-\zeta)\theta_B + 4K\langle AB\rangle, \tag{24}$$

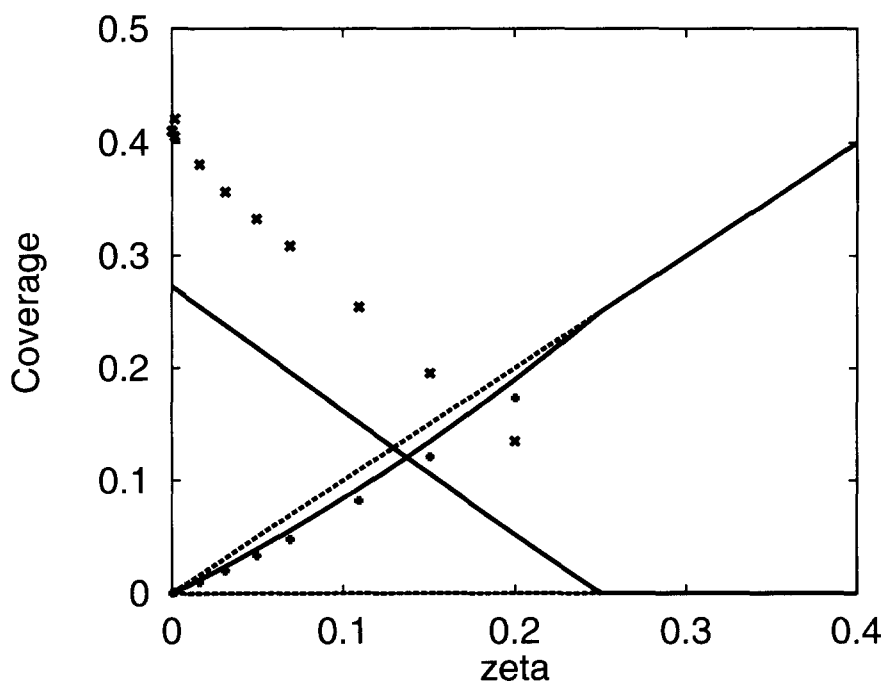

Fig. 5. The average coverages of A and B as a function of ζ determined by the mean-field approximation (dashed lines), the cluster approximation (solid lines), and Monte Carlo simulations (symbols). The coverage of B is an increasing function of ζ, whereas the coverage of A is a decreasing function.

$$\frac{d\langle AB\rangle}{dt} = \zeta\langle B*\rangle + 3K\langle AAB\rangle - 3K\langle BAB\rangle - K\langle AB\rangle - (1-\zeta)\langle AB\rangle, \quad (25)$$

$$\frac{d\langle AA\rangle}{dt} = 2\zeta\langle A*\rangle + 6K\langle AAB\rangle, \quad (26)$$

$$\frac{d\langle BB\rangle}{dt} = 2K\langle AB\rangle + 6K\langle BAB\rangle - 2(1-\zeta)\langle BB\rangle. \quad (27)$$

Here $\langle XY\rangle$ is the probability to find an Y to the right of an X at an arbitrary horizontal pair of neighboring sites. We have used

$$\langle XY\rangle = \langle YX\rangle = \langle \begin{matrix} X \\ Y \end{matrix} \rangle = \langle \begin{matrix} Y \\ X \end{matrix} \rangle,$$

and we have assumed that the three-site distributions are the same for straight and bent triplets of sites. Other two-site distributions than the ones found above can be determined by sum rules. We decouple the equations above by [23,44]:

$$\langle AAB\rangle = \frac{\langle AA\rangle\langle AB\rangle}{\theta_A}, \quad (28)$$

$$\langle BAB\rangle = \frac{\langle AB\rangle^2}{\theta_A}. \quad (29)$$

The steady state is then given by

$$\theta_A = 3\frac{4\zeta^2 - 5\zeta + 1}{12\zeta^2 - 11\zeta + 11}, \quad (30)$$

$$\theta_B = 4\zeta\frac{\zeta + 2}{12\zeta^2 - 11\zeta + 11} \quad (31)$$

if $\zeta \leq 1/4$ and $\theta_A = 0$, $\theta_B = \zeta$ if $\zeta \geq 1/4$ both in the limit $K \to \infty$, which is better than the mean-field result, but there are clearly still differences with the simulations results.

Mai et al. have argued that distributions with AB pairs should not be approximated [40]. In the limit $K \to \infty$ they become zero, but multiplied by K they may have some finite value. Instead rate equations of these so-called virtual distributions should be used to derive exact relations that express them in terms of nonvirtual distributions. Only the latter should be approximated. The results improve slightly with respect to Eqs. (30) and (31), but the difference vanishes in the limit $\zeta \to 0$. In fact the best agreement with the Monte Carlo simulations was obtained with the simple scheme $\langle AAB\rangle = \theta_A\langle AB\rangle$ and $\langle BAB\rangle = \theta_B\langle AB\rangle$.

The rate Eq. (23) and (24) are exact, but when taken alone seem not useful because of the presence of the term with $\langle AB\rangle$. We can, however, eliminate this distribution and arrive at the following exact relation for a steady state [74]:

$$\theta_A + \frac{1}{\zeta}\theta_B = 1. \quad (32)$$

When there are oscillations this relation still holds, provided we interpret the coverages as time-averaged coverages. This relation is an important guide to study the behavior of the Lotka model in the limit $\zeta \to 0$.

Fig. 6 shows how the coverages change as a function of time. We see clearly periodic oscillations. These had already been seen by Mai et al. [23]. Their correlation analysis predicted a Hopf-bifurcation from a stable equilibrium point to a limit cycle [37]. The Monte Carlo simulations do not show such a bifurcation, however. One only finds that the amplitude of the oscillations become smaller when ζ increases for a fixed grid size [74].

The amplitude of the oscillations also decreases when the grid size increases. This has been attributed by Mai et al. to the stochastic nature of the simulations [23]. Our interpretation is, on the other hand, that we are dealing with local oscillations, which are insufficiently coupled to yield global oscillations. This can be shown by doing simulations on a large grid and looking at only a small part of it. The results show that the amplitude of the oscillations in the small part is the same as the amplitude in a simulation with a small grid. When the local oscillations are not coupled they will oscillate out of phase, which leads to destructive interference and reduction of amplitude. Another indication that one sees essentially the same oscillations independent of grid size is that the power spectra of all simulations with the same ζ are identical except for a scaling of the peak heights.

The fact that the amplitude of the oscillations increases when ζ becomes smaller indicates that the synchronization mechanism that couples the local oscillations becomes more effective. The question therefore arises if there is a point at which the oscillations do become global. To answer this question we need information on the origin of the oscillations. We note in Fig. 6 that the oscillations consist of a sudden

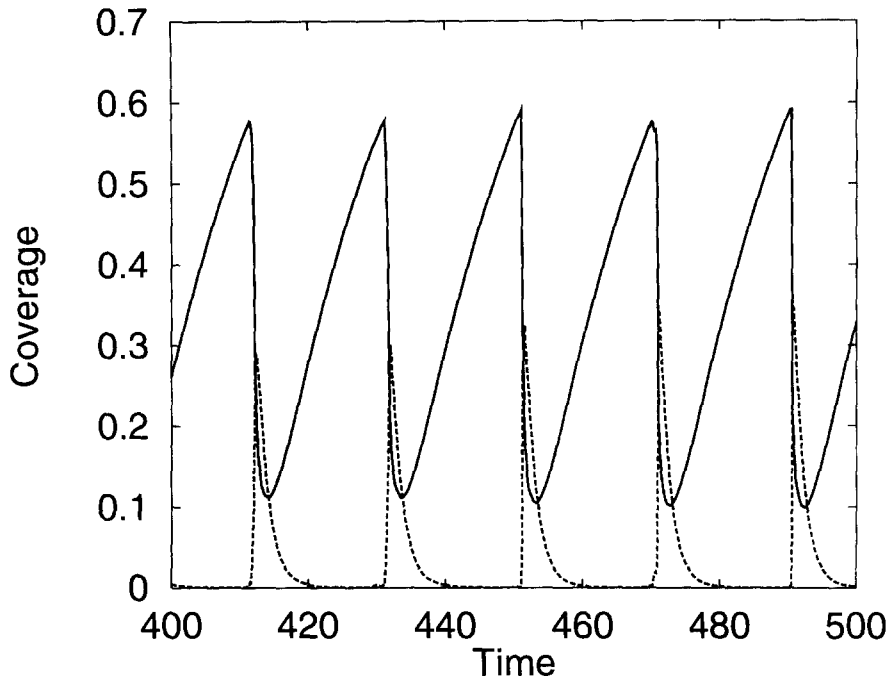

Fig. 6. The coverages of A (solid line) and B (dotted line) as a function of time. The data have been obtained from a Monte Carlo simulation of the Lotka model with ζ=0.05 on a 2048×2048 grid.

increase of θ_B and a corresponding decrease of θ_A, followed by a smooth decrease of θ_B and a smooth increase of θ_A. The fact that the sudden increase of θ_B and the decrease of θ_A are equal in size points to an avalanche of A+B→2B reactions as the cause of the oscillations. The decrease of θ_B is simply B desorption. As can be derived from Eq. (24) this decrease is exponential. The increase of θ_A is A adsorption, which has a more complicated time dependence, because the number of vacant sites changes due to A adsorption and B desorption.

The amplitude of the oscillations will increase when the size of the avalanches increases. We can define two average avalanche sizes. The average size $\langle s\rangle_{ads}$ per A adsorption is given by

$$\langle s\rangle_{ads} = \sum_{s=0}^{\infty} sP_{ads}(s), \tag{33}$$

where $P_{ads}(s)$ is the probability that an adsorption of A is immediately followed by an avalanche of size s. An avalanche of size s=0 means an adsorption of A on a site without neighboring B. As each A that adsorbs will disappear by participating in an avalanche that transforms it into a B, we have

$$\langle s\rangle_{ads} = 1. \tag{34}$$

Alternatively, one can look only at real avalanches; i.e., of size larger or equal to one. The average size $\langle s\rangle_{ava}$ of these is given by

$$\langle s\rangle_{ava} = \sum_{s=1}^{\infty} sP_{ava}(s), \tag{35}$$

where $P_{ava}(s)$ is the probability that an avalanche has size s. This probability is proportional to $P_{ads}(s)$. The proportionality constant can be derived from the normalization. We have $\sum_{s=0}^{\infty} P_{ads}(s) = 1$ and $\sum_{s=1}^{\infty} P_{ava}(s) = 1$, which leads to

$$P_{ava}(s) = \frac{P_{ads}(s)}{1 - P_{ads}(0)}. \tag{36}$$

From this we immediately get

$$\langle s\rangle_{ava} = \frac{1}{1 - P_{ads}(0)}. \tag{37}$$

If ζ is small, θ_B is small as well, and we may assume that all B's are well separated. In that case

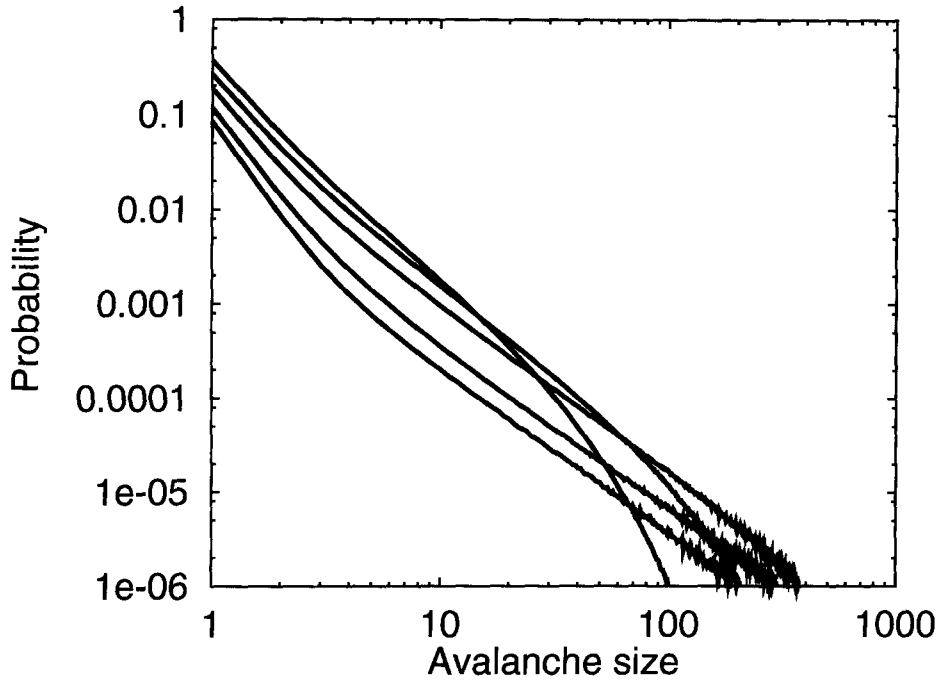

Fig. 7. Size distributions of avalanches in which A's are converted into B's. The data have been obtained from a Monte Carlo simulation of the Lotka model with ζ=0.05, 0.07, 0.11, 0.15, and 0.20 on a 2048×2048 grid.

$$P_{\mathrm{ads}}(0) = \frac{\theta_* - 4\theta_{\mathrm{B}}}{\theta_*}, \tag{38}$$

so that

$$\langle s \rangle_{\mathrm{ava}} = \frac{\theta_*}{4\theta_{\mathrm{B}}} = \frac{1-\zeta}{4\zeta}. \tag{39}$$

In the last step we have used Eq. (32). From this we see that for $\zeta \to 0$ the avalanche size diverges, which leads to global oscillations.

It is also quite interesting to take a closer look at the distribution of the size of the avalanches itself. It is clear that, if the size distribution is exponential (i.e. $P_{\mathrm{ava}}(s) \propto \exp(-s/\sigma)$), then $\langle s \rangle_{\mathrm{ava}}$ will be finite. This is not the case if we have a power law $P_{\mathrm{ava}}(s) \propto s^{-\tau}$ with $\tau \leq 2$. Fig. 7 shows that we have indeed such a power law. Discrepancies at small s have no effect on the divergence of $\langle s \rangle_{\mathrm{ava}}$. Those at large s are a consequence of a finite grid size, insufficient statistics due to a finite simulation time, and the fact that $\langle s \rangle_{\mathrm{ava}}$ only diverges for $\zeta \to 0$. The power law is, however, clearly visible. The exponent seems even independent on ζ.

The dimension two can be identified as the upper critical dimension for the Lotka model. Indeed, simulations on a three-dimensional cubic grid also show local oscillations for all ζ. On the other hand, simulations in one dimension show no oscillations. Instead one has a kinetic phase transition at $\zeta_{\mathrm{c}} \approx 0.24$, above which $\theta_{\mathrm{A}} < 1$ and below which $\theta_{\mathrm{A}} = 1$. At and above the critical dimension critical exponents can be obtained from the mean-field approximation [75]. That this is indeed the case can be seen with the help of Eq. (32). Mean field predicts that $\theta_{\mathrm{B}} \propto \zeta$, so that according to Eq. (32) θ_{A} need not become one at $\zeta = 0$. For dimensions two and three, $\theta_{\mathrm{A}} < 1$ for $\zeta \to \zeta_{\mathrm{c}}$ (=0), and $\theta_{\mathrm{B}} \propto \zeta$ as can be seen from the simulations. For dimension one $\theta_{\mathrm{A}} \to 1$ for $\zeta \to \zeta_{\mathrm{c}}$ and $\theta_{\mathrm{B}} \propto (\zeta - \zeta_{\mathrm{c}})$ with $\beta > 1$.

3.3. Comments on oscillations

A mean-field approach for, say, a chemical reaction involving two species (and thus two coupled nonlinear rate equations) can often lead to bistability. The presence of a third degree of freedom then allows a feedback path, which can lead to oscillations, quasi-

periodic or even chaotic solutions. In heterogeneous catalysis, the third degree of freedom can arise for several reasons. Known examples are the variations of the reactant adsorption rates due to adsorbate-induced surface reconstructions [8–10], adsorption to subsurface sites [76], and the blocking of adsorption sites through an inert adsorbate (discussed above). Other mechanisms are the coupling of the surface processes to pressure or temperature variations in the gas phase [77,78].

As elaborated above, while mean-field theory can in some cases give a qualitative way to discuss the dynamical transitions, it is usually quantitatively inaccurate. For example, mean-field theory can seriously overestimate the range of parameters where such effects occur. It can also turn a first-degree transition to a second-order one [79].

Bistability and oscillations can be regarded as to arise from a competition between two attractive fixed points in the phase space of the system. In mean-field theory the transition from one point to another occurs when the point looses its attractivity. However, in equilibrium statistical mechanics the (meta)stability of a phase in the coexistence region is governed by the rate of fluctuations. They nucleate a small region of the other phase and allow it to grow. Thus the region in parameter space where dynamical effects are observed is diminished when spatial fluctuations are included.

As a specific example, let us consider the case of CO oxidation on Pd and Pt surfaces. Several mechanisms for causing oscillations in this type of reactions have been suggested in the literature. For Pt surfaces, the oscillations observed at low pressures have been ascribed to changes in the oxygen sticking coefficient induced by surface reconstruction. At higher pressures oxide formation has been postulated as the dominant mechanism [80]. Stable oscillations and period doubling have been observed on Pd(1 1 0) [81]. They have been tentatively associated with the penetration of chemisorbed oxygen to the Pd bulk, experimentally proven by Ladas et al. [82]. Another experiment on Pd has shown none of the spatial structures observed for CO on Pt, presumably due to the homogenizing effect of gas-phase coupling [83]. A mean-field theory with subsurface oxygen changing the sticking coefficient of gas-phase oxygen reproduces the oscillations and the bifurcation. Successful modeling of the oscillations has been conducted by Imbihl et al. [77,84], and spatiotemporal patterns were shown to exist in this system [85]. There is also the observation that CO adsorption may trigger surface reconstruction on Pd, which may thus play a role as on Pt [86]. The mean-field theory results in oscillations between two non-oscillating steady states, while the observations indicate switching between two oscillating states. Thus there might be additional feedback mechanisms in producing the oscillations.

The question of the origin and nature of the oscillatory reactions is a complex one. In particular, the role of local correlations and fluctuations in affecting the stability, shape and period of oscillations is far from clear. It appears that careful and extensive Monte Carlo simulations are necessary to uncover the subtleties of oscillatory surface reactions.

4. Applications to realistic systems

4.1. Temperature-programmed desorption spectra

TPD is a very elegant method to determine kinetic parameters of surface processes, but, although the experiment is conceptually very simple, the interpretation of the spectra often is not. A nice review with older Monte Carlo work on TPD has been written by Lombardo and Bell [24]. The drawback of the work presented in that review is the fact that the time dependence of the simulations is not correct. The explicit time dependence is especially important for simulating TPD, because without a correct temporal scaling spectra taken with different heating rates cannot be compared. The problem of the correct time dependence in Monte Carlo simulations of TPD has first been addressed by Meng and Weinberg [28] following a more general study by Fichthorn and Weinberg [27]. We have developed a method in which times, at which reactions occur, are generated according to a probability distribution for them [25]. For time-independent reaction rate constants this is a well-known and simple method [29,30]. The probability distributions are exponentials. In TPD the rate constants are no longer constant, and the probability distributions are more complicated.

Monatomic desorption without lateral interactions is a simple process; the TPD spectrum can even be calculated analytically [25]. When lateral interactions

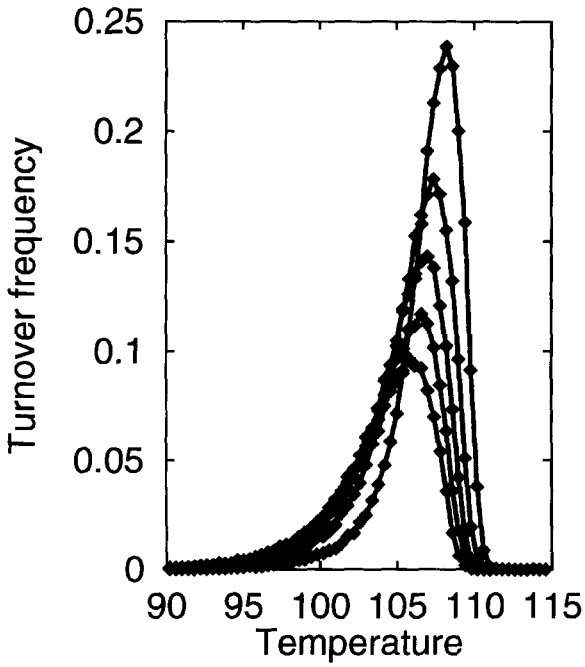

Fig. 8. TPD spectra showing the desorption rate (in units of the number of Xe atoms per second per site) as a function of the temperature (in K) for heating rate B=1 K s^{-1}. The dots are results directly from the MC simulations, and the lines connect MC results with the same initial coverage. The five curves are from left to right for initial coverage 0.598, 0.698, 0.806, 0.906 and 1.000.

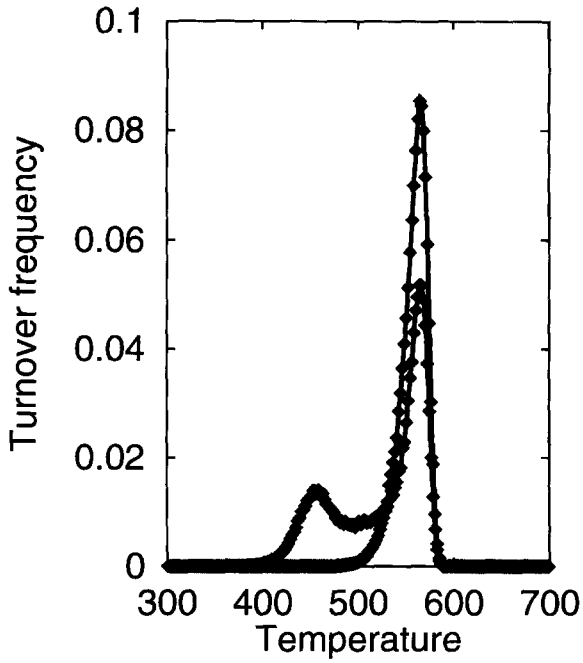

Fig. 9. TPD spectra showing the desorption rate (in units of the number of K atoms/CO molecules per second per site) as a function of the temperature (in K) for heating rate B=2.5 K s^{-1}. The dots are results directly from the MC simulations, and the lines connect MC results with the same initial coverage. The curve with just one peak is CO, and the curve with two peaks is potassium.

are included the interpretation of the TPD spectra becomes difficult. Experimentally the spectra of Xe/Pt(1 1 1) seem of order zero [87], with the order of the process signifying the power-law coverage dependence of the desorption rate. It is determined as the logarithmic derivative of the rate with respect to the coverage. A molecular dynamics study suggested that for Xe on Pt the low order of the process might be caused by attractive Xe–Xe interactions [88]. A Monte Carlo study on the influence of attractive interactions on TPD spectra showed that even small interactions can change the apparent order of the desorption substantially, and can even make it negative [89]. The results of a Monte Carlo simulation of Xe/Pt(1 1 1) is shown in Fig. 8.

A comparison with experiments indicates that the situation is more complicated than one would expect. Lateral interactions have two effects. First, they determine the structure of the adlayer. Attractive interactions lead to island formation at low temperatures. Second, they determine the rate of desorption, which will be dependent on the number of neighbors. If the second effect is negligible, the first is irrelevant. If the first effect is negligible and the adsorbates are distributed randomly over the surface, the second effect changes the order maximally. In Xe/Pt(1 1 1) both effects are present. The net result is that the order of the desorption is about zero, and some short-range order can be observed [89].

A nice example of the power of Monte Carlo simulations is the prediction that repulsive lateral interactions can lead to multiple-peak spectra [24]. This is because, after adsorbates with many neighbors have desorbed, the remaining adsorbates have few neighbors and are bound to the surface stronger, and will only desorb at much higher temperatures. A combination of attractive and repulsive interactions is found in K+CO/Co(0 0 0 1) [90]. The simulated spectra shown in Fig. 9 show two potassium peaks and one CO peak at the same temperature as the higher

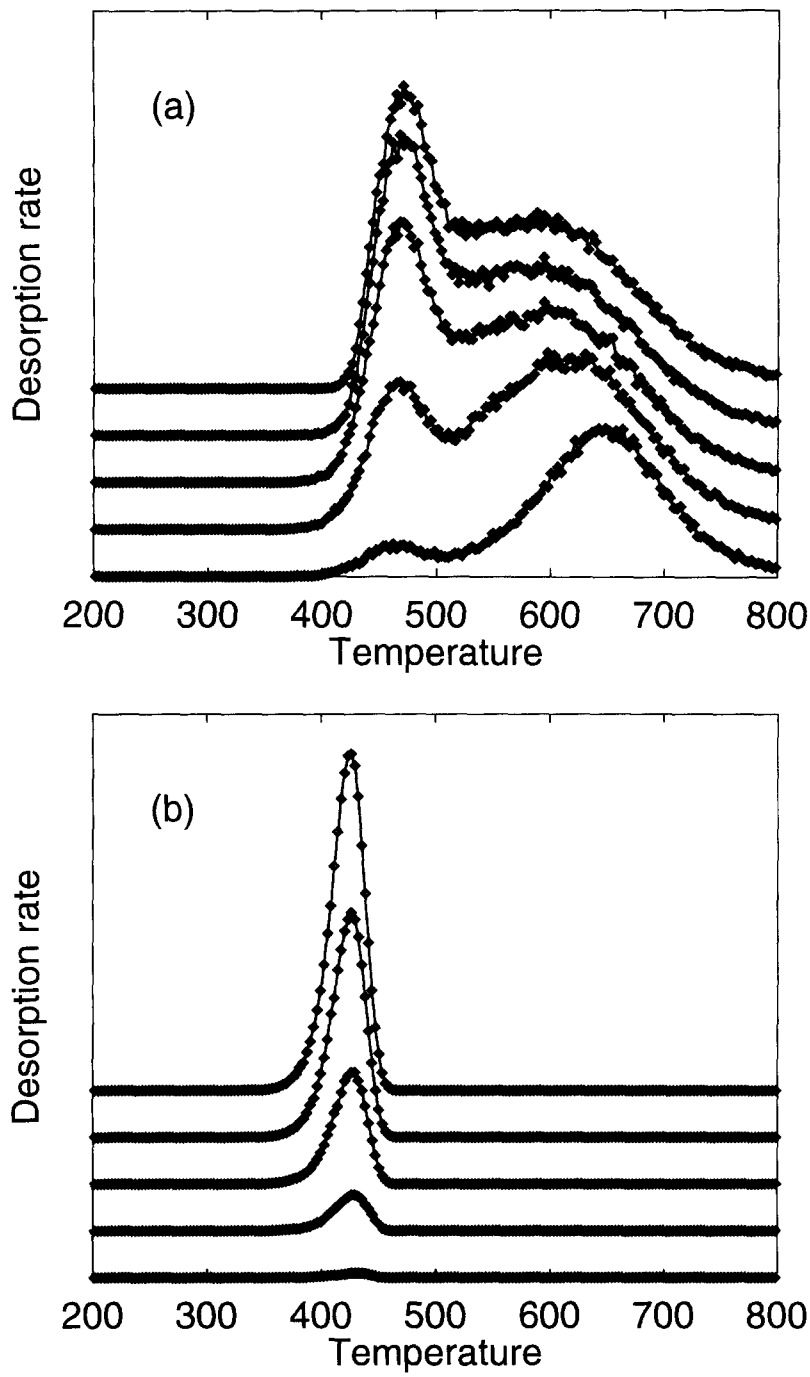

Fig. 10. TPD spectra showing the desorption rate in arbitrary units of N_2 (a) and NO (b). The symbols are results directly from the Monte Carlo simulations and the lines connect Monte Carlo results with the same initial coverage. The curves are for initial NO coverages 0.489, 0.401, 0.303, 0.202 and 0.102. They have been offset for clarity.

potassium peak. The explanation for the spectra is that the K–K interaction is repulsive, which leads to two peaks. The reason why the CO peak and one potassium peak are at the same temperature is that there is an attractive K–CO interaction. Desorption of one adsorbate decreases the activation energy for desorption of the other, so that it desorbs following immediately the desorption of the first.

TPD experiments with reactions occurring on the surface are often called temperature-programmed reaction experiments. An example is the reduction of NO on Rh(1 1 1) [91]. At low temperatures NO is stable, but when the temperature is increased it dissociates. At low initial coverages only desorption on N_2 and O_2 is observed. At high initial coverages, however, also NO is seen. Simulated spectra are shown in Fig. 10. The reason why not all NO dissociates is that at high coverages oxygen and nitrogen atoms that have been formed block sites for further dissociation. The system, however, is more complex than that. There are strong repulsive lateral interactions that limit the number of neighboring sites that can be occupied, and which are known to lead to complicated adlayer structures for Ni(1 1 1) [92–94]. In the simulations we have tried to describe only the short-range order correctly. This is sufficient even to get the correct TPD spectrum of N_2. There is a second-order peak as one expects, but also a peak at lower temperature which seems first-order. This peak is caused by the nitrogen atoms that are formed from NO that only dissociates after sites become vacant because of NO desorption. These atoms are formed next to nitrogen atoms that originate from NO that has dissociated at low temperatures. This reduces the order for N_2 desorption by one. The simulated spectra in Fig. 10 agree well with the experimental spectra.

4.2. CO hydrogenation on model catalysts

While the focus of Monte Carlo techniques in simulations of surface reactions has mainly been in their generic critical and kinetic behavior, the method is a potentially powerful tool in detailed studies of complex reaction systems. When combined with experimental studies, the techniques can uncover the key microscopic factors controlling the overall reactivity and product distributions. The techniques are flexible; new reaction steps, surface structures and ensemble effects can easily be incorporated. Promising results have been reported, for example, for CO oxidation on Pt [9], for NO–CO reactions on Pd and Pt [95], as well as in an earlier study of N_2 chemisorption on Ru [96].

As a specific example, we discuss here the complex case of CO hydrogenation on cobalt [26,97]. This reaction has been studied experimentally, and data on the product distributions as a function of the partial reactant pressures is available [98,99]. The main reaction steps are the adsorption of reactants, either molecular or dissociative, the diffusion of hydrogen, the sequence of hydrocarbon reactions and water formation, and the desorption of reaction products. The most striking feature of the experiments is the negative slope of the methane production rate as a function of the CO partial pressure (see Fig. 13 below).

The catalyst surface is modeled by a hexagonal lattice to model the (0 0 0 1) face of a h.c.p. or the (1 1 1) face of an f.c.c. metal. Different lattice sites for C, O and their compounds (site A) and for H (site B) are assumed, as schematically shown in Fig. 11. An essential feature is that CO and H_2 do not compete for the same sites – a conclusion necessary for obtaining a reactive steady state for a wide range of partial pressures (as in experiments) rather than saturating the surface with CO or H.

The simulations are carried out under constant pressure conditions, so that the total pressure of the mixture is scaled to one by adding an inert fill-up component, such as gaseous Ar. The partial pressures of CO and H_2 are then the essential variables. Indeed, the dependence of the turnover on the CO partial pressure is the major challenge, as the dependence on H_2 partial pressure can quite easily be reproduced for quite a large set of parameter values.

Hydrogen is assumed to adsorb dissociatively, and thus requires two neighboring B sites. CO adsorbs to an A site, and can dissociate with a finite probability if there is an adjacent vacant A site. In the basic algorithm (see Fig. 12), no CO desorption or diffusion is allowed, while hydrogen can diffuse. These assumptions can easily be altered and new steps included (see below).

The surface reactions are modeled by invoking the carbide mechanism. It contains four features:

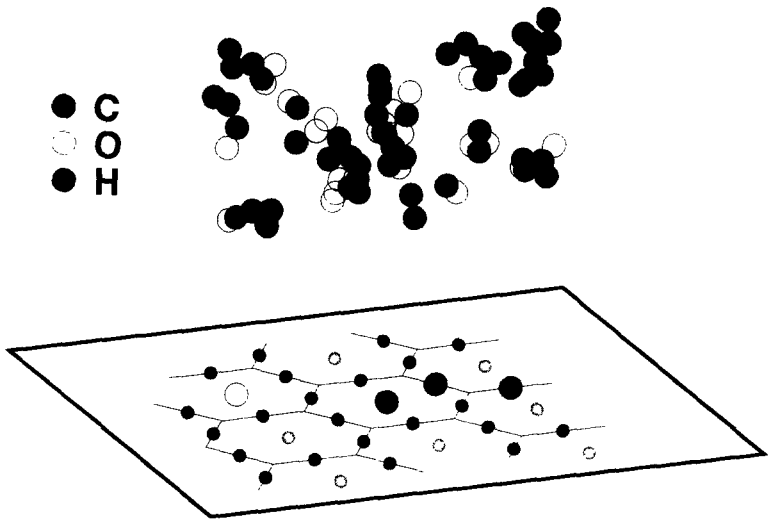

Fig. 11. A schematic picture of the catalytic CO hydrogenation reaction. The adsorption sites for CO (light small circles) form a hexagonal lattice. Between the CO sites there is an adsorption site for hydrogen (full small circles). Argon atoms, which are used as a fill-up gas to keep the total pressure constant, are not shown.

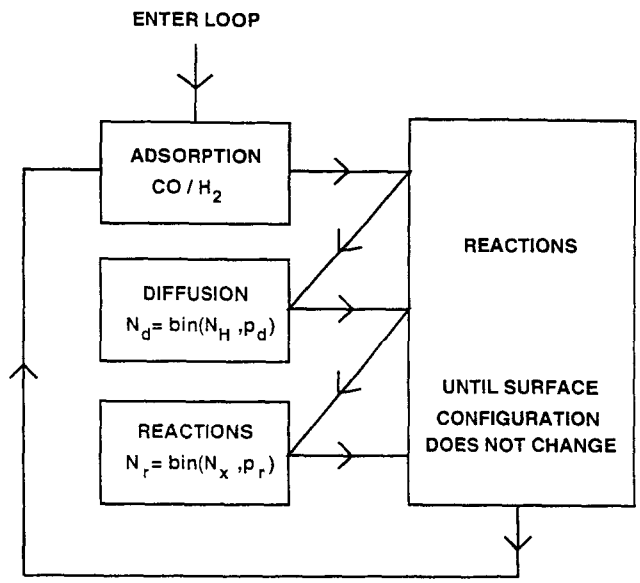

Fig. 12. The main simulation loop for CO hydrogenation. The numbers of atoms/molecules reacting or diffusing (N_r, N_d) is calculated from the binomial distribution using the number of corresponding species on the surface (N_x) and the corresponding reaction probability per unit time.

(1) Methane is formed via stepwise hydrogenation of carbon through nearest-neighbor reactions

$$C(ads) + H(ads) \rightarrow CH(ads) + *, \quad (40)$$

$$CH(ads) + H(ads) \rightarrow CH_2(ads) + *, \quad (41)$$

$$CH_2(ads) + H(ads) \rightarrow CH_3(ads) + *. \quad (42)$$

$$CH_3(ads) + H(ads) \rightarrow CH_4(gas) + 2*. \quad (43)$$

Methane desorbs immediately from the surface.

(2) Hydrocarbon chains grow by addition of CH_2 groups to the alkyl species

$$C_nH_{2n+1}(ads) + CH_2(ads) \rightarrow C_{n+1}H_{2n+3}(ads) + *. \quad (44)$$

(3) The hydrocarbon chains terminate through either by α-hydrogenation

$$C_nH_{2n+1}(ads) + H(ads) \rightarrow C_nH_{2n+2}(gas) + 2*. \quad (45)$$

producing alkanes, or by β-dehydrogenation

$$C_nH_{2n+1}(ads) \rightarrow C_nH_{2n}(gas) + H(ads), \quad (46)$$

producing alkenes. In the latter case the adsorbed hydrogen remains on the A-site until it participates with further reactions with its neighbor or diffuses to a new B-site.

(4) Water is formed from the adsorbed hydrogen and oxygen.

$$O(ads) + H(ads) \rightarrow OH(ads) + *, \quad (47)$$

$$OH(ads) + H(ads) \rightarrow H_2O(gas) + 2*. \quad (48)$$

Each surface reaction has an associated reaction probability, which now can be varied to identify the rate-limiting steps. To facilitate the simulation, a set of default values for the parameters is specified and the effects of various mechanisms are then simulated individually. The simulations usually start from an empty lattice with 100×100 A-sites and periodic boundary conditions. Typically a few million time steps are used to obtain steady states; the product distributions and coverages are then obtained by averaging over another few million time steps.

During the simulation runs, surface reactions can be initiated by any change in the configuration of the adsorption sites, for example through adsorption or diffusion. This can then trigger an avalanche of reactions on the surface. Because every reaction involves at least one A site, the changed sites are stored and the reaction followed until it stops either by running out of suitable nearest-neighbor reactive pairs or by 'getting stuck' at a low-probability reaction step. In the latter case, it will continue later with a given probability.

Once the model has been specified, one can systematically scan the available phase space and sort out the relevant, qualitative features of the reaction system.

By varying the parameters systematically in the Monte Carlo simulations and comparing with experimental product distributions, it is possible to draw several conclusion on the Fischer–Tropsch synthesis on cobalt:

1. H and CO occupy different adsorption sites.
2. The rate-limiting step is α-hydrogenation.
3. Hydrogen diffuses fast.
4. The rate for β-dehydrogenation is lower than that for α-hydrogenation.
5. The hydrocarbon chain growth is slow compared to the majority of surface reactions.
6. The potential barrier for CO dissociation is low.
7. Water removal is relatively fast.

Fig. 13 shows a comparison between the results of Monte Carlo simulations outlined above and the experimental turnover rates when the CO partial pressure in the reaction chamber is varied. The Monte Carlo simulations of this section work with Monte Carlo instead of real time, so a scaling of the rate constants has been done so that the simulation time unit can be connected to real physical time. The simulation results show partial pressure dependencies similar to those observed in the experiments, especially for methane and ethene. While there is fair overall agreement between the simulations and the experiments, some discrepancies remain. The selectivity towards methane is too small, and there are some systematic deviations of the rate of formation of longer chains, especially at low CO pressures.

This suggests the idea of introducing additional aspects into the Monte Carlo model. These include the reduction of CoO

$$CO(ads) + Co \rightarrow C(ads) + CoO, \quad (49)$$

$$CoO + H(ads) \rightarrow Co + OH(ads), \quad (50)$$

instead of or in addition to CO dissociation on the surface. The latter equation is expected to be slow, and when replacing the first step of water formation could become another rate-limiting step. Other possible new features include the reverse reaction (CH(ads) dissociation)

$$CH(ads) + * \rightarrow C(ads) + H(ads), \quad (51)$$

and desorption of CO and/or H from the surface.

Recently, Liu et al. have extended the Monte Carlo simulations to contain these additional features [100]. They conclude that, as first suggested by the experimental work of Lahtinen et al. [99], CoO reduction does indeed increase the selectivity towards producing

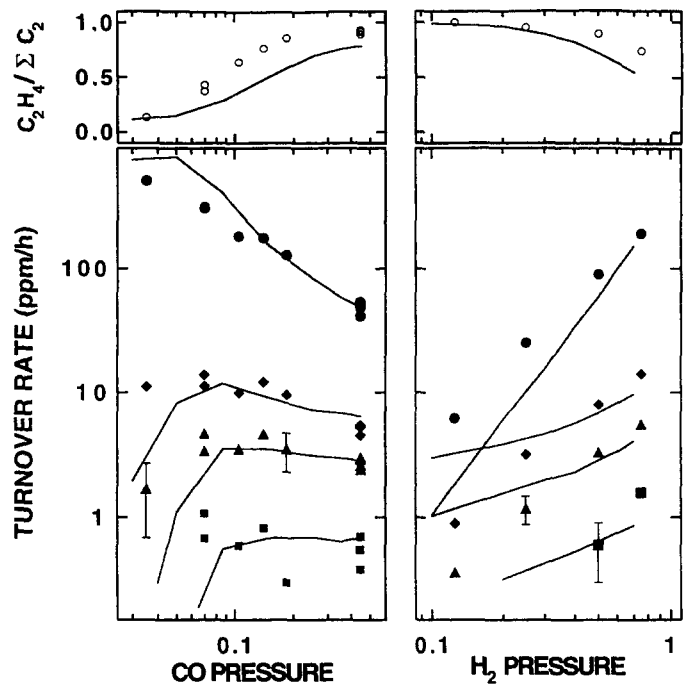

Fig. 13. Comparison of the partial pressure dependencies between the simulated hydrocarbon formation and the experimental data at 525 K and 101 kPa [98,99]. The fraction of ethene in the C_2 products (top) and the turnover rates of C_1–C_4 hydrocarbons (main chart) are shown as a function of CO and H_2 partial pressure. The simulated results are shown by solid lines and the markers denote experimental points: ethene fraction (open circles), C_1 (closed circles), C_2 (diamonds), C_3 (triangles), and C_4 (squares). The simulated data is normalized by a factor to connect the simulation timestep to real time. The probabilities for α- and, β-hydrogenation are 10^{-5} and 10^{-6}, respectively. The unit time probability for chain growth is 10^{-4} and that for hydrogen diffusion 10^{-3}. The effective relative sticking coefficients for CO and H_2 are 0.08 and 1.0, respectively. From Ref. [26].

methane while maintaining the negative slope of the CO partial pressure dependence. It blocks the hydrocarbon chain growth and curbs hydrogen adsorption, thus increasing the selectivity towards methane. While additional experimental studies to confirm the presence of this step are called for, it seems quite possible that it plays a role. On the other hand, the dissociation of CH(ads) and the desorption of either CO or H do not seem to be important for understanding the product distributions.

The detailed studies of the complex problem of CO hydrogenation on a cobalt catalyst demonstrate the value of Monte Carlo simulations for analyzing the irreversible kinetics of nonequilibrium steady states such as those encountered in heterogeneous catalysis. Model building is straightforward and flexible. The major limitations arise from computational limitations. Proper attention should be placed to finite-size effects, especially when considering absolute reactivities, critical properties or oscillatory behavior. Complicated reaction sequences with several rate-limiting steps can also become very time-consuming. In this case algorithms modified from the straightforward sequential Monte Carlo methods can be considered. One interesting possibility is to combine mean-field and lattice-gas type treatments in a hybrid scheme. Tammaro et al. [101] have introduced such techniques to study spatiotemporal behavior in a system with coexisting immobile and highly mobile reactants.

5. Future directions

The Monte Carlo simulations for discrete, irreversible nonequilibrium systems as described above offer a conceptually simple yet powerful method to study complex phenomena. With computer power rapidly becoming ever more affordable, such simula-

tion tools can be extended to cover wide classes of phenomena.

From the statistical physics point of view, however, much remains to be done to solidify the basis of understanding the behavior of such systems. For example, the classification of nonequilibrium phase transitions is far from complete. The critical behavior of several kinetic model falls into the category of directed percolation or equivalently Reggeon field theory [102]. Variants of this basic model include several adsorption-reaction models [103–106], kinetic Ising models [42,107], and the driven diffusive lattice gas [108]. The question then immediately arises as what are the key factors affecting the critical behavior: conservation laws, internal symmetries of the model, or details of reaction laws? What role does the spatial dimensionality play? It is obvious that sophisticated analytic methods such as those based on field theory are needed to ultimately clarify the picture of universality classes for nonequilibrium phase transitions.

Another important consideration is the behavior of the systems at larger length and time scales. While simulations are constantly improving, the efficiency of these techniques will always be ultimately limited by the necessity to very large lattice sizes either to reduce statistical noise or to attack the behavior at a scale much larger than the microscopic (atomic) scale. Indeed, a potentially serious limitation of the techniques discussed above is the computational difficulty in dealing with multiple and vastly varying length and time scales.

In this respect, the simulations would obviously be much more effective if one could coarse-grain the system and treat regions of adsorption sites on the surface as a single collective coordinate. This would greatly facilitate the examination of both the large-length scale and low-frequency dynamic behavior of the models.

One possibility to carry out such coarse-graining near a phase transition is to apply renormalization-group analysis to the Master Equation. Near the phase transition, the relaxation rate to towards the steady state is governed by the smallest eigenvalue of steady state equation and the system size. Thus the relevant critical exponents can be found through the behavior of the low-lying modes of densities and correlation functions as a function of system size. The challenge is thus basically a numerical renormalization-group analysis of the Master Equation, now in the context of a nonequilibrium system.

For several problems in heterogeneous catalysis, the flow conditions in the reactor and on the surface are crucial. Again, one can imagine coupling the reactant flows to the surface reactivity through coarse-graining. A 'mesoscopic' area of the surface (say, 100×100 sites) would be assigned values of the macroscopic variables of gas pressures, velocities and temperature. The steady-state reaction conditions for this cell would then be determined through the Monte Carlo procedures discussed in the previous chapters. Moreover, to account for the macroscopic fluid flow the cell would be coupled to similarly defined neighboring cells. The coupling would be made by invoking the lattice-gas or cellular-automaton implementations of fluid dynamics [109]. One would then have conceptually similar schemes for describing both the reactivities of the cells at the surface and the fluid dynamics in the chamber. The physical time scales for the two are obviously very different. However, they can be computationally handled by intervening Monte Carlo runs for the two subsystems. Reactive flows can also be easily implemented to obtain a global description of the reactor [110]. While such schemes have not yet been attempted, the recent progress in lattice-gas models for complicated flow problems make this approach interesting as well.

One possibility to improve the efficiency of Monte Carlo simulation methods is to exploit the inherent parallelism in the problem also in its computational implementation. Parallel machines are becoming increasingly more popular and promise true upwards scalability in their performance. The potential success of efficiently implementing the simulation techniques discussed above to parallel computer architectures hinges on the possibility of mapping the Monte Carlo models to cellular automata with local dynamical rules. Individual cells or groups of cells could then be assigned to different processors, which would only communicate with their neighbors.

There have been several efforts to simulate surface reactions with cellular automaton techniques. These include studies of the ZGB-model [111,112], including CO diffusion [113] and NH_3 formation [114]. However, it is important to design the algorithm so that the stoichiometry and/or kinetic rules are correctly preserved, as the results, in particular the critical

properties, seem to depend on the actual implementation.

As a final remark, one can list the long-standing hope of being able to independently determine the microscopic probabilities embedded in the Monte Carlo scheme, either from electronic structure calculations or from separate surface-science experiments. Such a capability would obviously reduce the number of unknown parameters and would help in identifying the important reaction mechanisms and the global bottlenecks. However, quantitative calculations of reaction rates and activated processes are notoriously difficult. Although some calculations of rate constants of surface reactions have been published [115,116], at this point one usually has to settle with relatively crude estimates.

Acknowledgements

We are grateful for Dr. J.-P. Hovi for a critical reading of the manuscript.

References

[1] A.A. Ovchinnikov and Ya.B. Zeldovich, Chem. Phys., 28 (1978) 214.
[2] D. Rand, S. Ostlund, J. Sethna and E. Siggia, Phys. Rev. Lett., 49 (1982) 132.
[3] E. Abraham and S.D. Smith, Rep. Prog. Phys., 45 (1982) 815.
[4] B. Chance, E.K. Pye, A. Ghosh and B. Hessi (Eds.), Biological and Biochemical Oscillations, Academic Press, New York, 1973.
[5] P. Bak, C. Tang and K. Wiesenfeld, Phys. Rev. Lett., 59 (1987) 381.
[6] B.S. Kerner and P. Konhäuser, Phys. Rev. E, 48 (1993) 2335.
[7] G.F. Mazenko, Phys. Rev. Lett., 63 (1989) 1605.
[8] P. Møller, K. Wetzel, M. Eiswirth and G. Ertl, J. Chem. Phys., 85 (1986) 5328.
[9] G. Ertl, Science, 254 (1991) 1750.
[10] M. Eiswirth, K. Krischer and G. Ertl, Surf. Sci., 202 (1988) 565.
[11] Th. Fink, J.-P. Dath, R. Imbihl and G. Ertl, J. Chem. Phys., 95 (1991) 2109.
[12] G. Veser and R. Imbihl, J. Chem. Phys., 96 (1992) 7155.
[13] S.J. Lombardo, T. Fink and R. Imbihl, J. Chem. Phys., 98 (1993) 5526.
[14] B. Kasemo, K.-E. Keck and T. Högberg, J. Catal., 66 (1980) 441.
[15] B. Kasemo and K.-E. Keck, Surf. Sci., 167 (1986) 313.
[16] E.M. Lifshitz and L.P. Pitaevskii, Physical Kinetics, Pergamon Press, Oxford, 1981.
[17] I. Langmuir, Chem. Rev., 65 (1929) 451.
[18] V.P. Zhdanov, Elementary Physicochemical Processes on Solid Surfaces, Plenum, New York, 1991.
[19] V.N. Kuzovkov and E. Kotomin, Rep. Prog. Phys., 51 (1988) 1479.
[20] H.C. Kang and W.H. Weinberg, Surf. Sci., 299/300 (1994) 755.
[21] K. Binder and D.W. Heermann, Monte Carlo Simulation in Statistical Physics, 2nd ed., Springer, Heidelberg, 1992.
[22] R.M. Ziff, E. Gulari and Y. Barshad, Phys. Rev. Lett., 56 (1986) 2553.
[23] J. Mai, V.N. Kuzovkov and W. von Niessen, preprint.
[24] S.J. Lombardo and A.T. Bell, Surf. Sci. Rep., 13 (1991) 1.
[25] A.P.J. Jansen, Comput. Phys. Comm., 86 (1995) 1.
[26] J.-P. Hovi, J. Lahtinen, Z.S. Liu and R.M. Nieminen, J. Chem. Phys., 102 (1995) 7674.
[27] K.A. Fichthorn and W.H. Weinberg, J. Chem. Phys., 95 (1991) 1090.
[28] B. Meng and W.H. Weinberg, J. Chem. Phys., 100 (1994) 5280.
[29] K. Binder, in: K. Binder (Ed.), Monte Carlo Methods in Statistical Physics, Topics in Current Physics, Springer, Berlin, 1986.
[30] J. Honerkamp, Stochastische Dynamische Systeme, VCH, Weinheim, 1990.
[31] G.A. Somorjai, Introduction to Surface Chemistry and Catalsis, Wiley, Chichester, 1993.
[32] F.C. Alcaraz, M. Droz, M. Henkel and V. Rittenberg, Ann. Phys., 230 (1994) 250.
[33] J.-P. Hovi, Master's Thesis, Helsinki University of Technology, 1993, unpublished.
[34] R.M. Ziff and B.J. Brosilow, Phys. Rev. A, 46 (1992) 4630.
[35] V.P. Zhdanov and B. Kasemo, Surf. Sci. Rep., 20 (1994) 111.
[36] A.P.J. Jansen and R.M. Nieminen, J. Chem. Phys., 106 (1997) 2038.
[37] J. Hale and H. Koçak, Dynamics and Bifurcations, Springer, New York, 1991.
[38] M.M. Slin'ko and N.I. Jaeger, Oscillating heterogeneous catalytic systems, Stud. Surf. Sci. Catal. 86 (1994).
[39] J. Mai, V.N. Kuzovkov and W. von Niessen, Physica A, 203 (1994) 298.
[40] J. Mai, V.N. Kuzovkov and W. von Niessen, J. Chem. Phys., 100 (1994) 6073.
[41] L.D. Landau and E.M. Lifshitz, Statistical Physics Part 1, Course of Theoretical Physics, vol. 5, Pergamon Press, Oxford, 1980.

[42] R.J. Glauber, J. Math. Phys., 4 (1963) 294.
[43] J.G. Kirkwood, J. Chem. Phys., 3 (1935) 300.
[44] J. Mai, V.N. Kuzovkov and W. von Niessen, J. Chem. Phys., 100 (1994) 8522.
[45] J. Mai, W. von Niessen and A. Blumen, J. Chem. Phys., 93 (1990) 3685.
[46] H.-P. Kaukonen and R.M. Nieminen, J. Chem. Phys., 91 (1989) 4380.
[47] M. Ehsasi, M. Matloch, J.H. Block, K. Christmann, F.S. Rys and W. Hirschwald, J. Chem. Phys., 91 (1989) 4949.
[48] P. Araya, W. Porod, R. Sant and E.E. Wolf, Surf. Sci., 208 (1989) L80.
[49] P. Fischer and U.M. Titulaer, Surf. Sci., 221 (1989) 409.
[50] P. Dufour, M. Dumont, V. Chabart and J. Lion, Comput. Chem., 13 (1989) 25.
[51] M. Dumont, P. Dufour, B. Sente and R. Dagonnier, J. Catal., 122 (1990) 95.
[52] P. Smilauer and V. Matolin, Prog. Surf. Sci., 35 (1990) 193.
[53] E.V. Albano, Appl. Phys. A, 55 (1992) 226.
[54] J.W. Evans, J. Chem. Phys., 97 (1992) 572.
[55] B.J. Brosilow and R.M. Ziff, Phys. Rev. A, 46 (1992) 4534.
[56] M.W. Deem, W.H. Weinberg and H.C. Kang, Surf. Sci., 276 (1992) 99.
[57] Y. Boudeville and E.E. Wolf, Surf. Sci., 297 (1993) L127.
[58] T. Tome and R. Dickman, Phys. Rev. E, 47 (1993) 948.
[59] I. Jensen and H.C. Fogedby, Phys. Rev. A, 42 (1990) 1969.
[60] J. Mai, V.N. Kuzovkov and W. von Niessen, J. Chem. Phys., 98 (1993) 10017.
[61] L.V. Lutsevich, V.I. Elokhin, A.V. Myshlyavtsev, A.G. Usov and G.S. Yablonskii, J. Catal., 132 (1991) 302.
[62] J.W. Evans, J. Chem. Phys., 98 (1993) 2463.
[63] D.S. Sholl and R.T. Skodje, Surf. Sci., 334 (1995) 295.
[64] J. Mai and W. von Niessen, Chem. Phys., 156 (1991) 63.
[65] M. Tammaro and J.W. Evans, Phys. Rev. E, 52 (1995) 2310.
[66] J.J. Luque, F. Jimenez-Morales and M.C. Lemos, J. Chem. Phys., 96 (1992) 8535.
[67] J. Satulovshy and E.V. Albano, J. Chem. Phys., 97 (1993) 9440.
[68] M.H. Kim and H. Park, Phys. Rev. Lett., 73 (1994) 2579.
[69] J. Köhler and D. Ben-Avraham, J. Phys. A, 25 (1992) L141.
[70] J.-P. Hovi, J. Vaari, H.-P. Kaukonen and R.M. Nieminen, Comput. Mater. Sci., 1 (1992) 33.
[71] J. Mai, A. Casties, W. von Niessen and V.N. Kuzovkov, J. Chem. Phys., 102 (1995) 5037.
[72] L.V. Lutsevich, V.I. Elokhin, S.V. Ragozinskii and G.S. Yablonskii, J. Catal., 142 (1993) 198.
[73] R.J. Gelten, J.P.L. Segers, J.J. Lukkien, P.A.J. Hilbers, A.P.J. Jansen and R.A. van Santen, in preparation.
[74] J.-P. Hovi, A.P.J. Jansen and R.M. Nieminen, Phys. Rev. E, 55 (1997) 4170.
[75] S.K. Ma, Modern Theory of Critical Phenomena, Benjamin, Reading, 1976.
[76] D.G. Vlachos, L.D. Schmidt and R. Aris, J. Chem. Phys., 93 (1990) 8306.
[77] M.R. Bassett and R. Imbihl, J. Chem. Phys., 93 (1990) 811.
[78] Y. Kuramoto, Chemical Oscillations, Waves, and Turbulence, Springer, Heidelberg, 1984.
[79] P. Grassberger, Z. Phys. B, 47 (1982) 365.
[80] J.E. Turner, B.C. Sales and M.B. Maple, Surf. Sci., 103 (1981) 54.
[81] M. Ehsasi, C. Seidel, H. Ruppender, W. Drachsel, J.H. Block and K. Christmann, Surf. Sci., 210 (1989) L198.
[82] S. Ladas, R. Imbihl and G. Ertl, Surf. Sci., 219 (1989) 88.
[83] M. Ehsasi, O. Frank and J.H. Block, Chem. Phys. Lett., 165 (1990) 115.
[84] N. Hartmann, K. Krischer and R. Imbihl, J. Chem. Phys., 101 (1994) 6717.
[85] M. Berdau, M. Ehsasi, A. Karpowicz, W. Engel, K. Christmann and J.H. Block, Vacuum, 45 (1994) 271.
[86] R. Raval, S. Haq, M.A. Harrison, G. Blyholder and D.A. King, Chem. Phys. Lett., 167 (1990) 391.
[87] H.R. Siddiqui, P.J. Chen, X. Guo and J.T. Yates Jr., J. Chem. Phys., 92 (1990) 7690.
[88] A.P.J. Jansen, J. Chem. Phys., 97 (1992) 5205.
[89] A.P.J. Jansen, Phys. Rev. B, 52 (1995) 5400.
[90] J. Vaari, J. Lahtinen, T. Vaara and P. Hautojärvi, Surf. Sci., 346 (1996) 1.
[91] H.J. Borg, J.F.C.-J.M. Reijerse, R.A. van Santen and J.W. Niemantsverdriet, J. Chem. Phys., 101 (1994) 10052.
[92] S. Aminpirooz, A. Smalz, L. Becker and J. Haase, Phys. Rev. B, 45 (1992) 6337.
[93] N. Materer, A. Barbieri, D. Gardin, U. Starke, J.D. Batteas, M.A. Van Hove and G.A. Somorjai, Phys. Rev. B, 48 (1993) 2859.
[94] N. Materer, A. Barbieri, D. Gardin, U. Starke, J.D. Batteas, M.A. Van Hove and G.A. Somorjai, Surf. Sci., 303 (1994) 319.
[95] B. Meng, W.H. Weinberg and J.W. Evans, J. Chem. Phys., 101 (1994) 3234.
[96] E.S. Hood, B.H. Toby and W.H. Weinberg, Phys. Rev. Lett., 55 (1985) 2437.
[97] J.-P. Hovi, J. Lahtinen, J. Vaari and R.M. Nieminen, Surf. Sci., 311 (1994) 331.
[98] J. Lahtinen, T. Anraku and G.A. Somorjai, J. Catal., 142 (1993) 206.
[99] J. Lahtinen, T. Anraku and G.A. Somorjai, Catal. Lett., 25 (1994) 241.
[100] Z.S. Liu, Licentiate Thesis, Helsinki University of Technology, 1995, unpublished.
[101] M. Tammaro, M. Sabella and J.W. Evans, J. Chem. Phys., 103 (1995) 1.
[102] H.K. Janssen, Z. Phys. B, 42 (1981) 151.
[103] D.A. Browne and P. Kleban, Phys. Rev. A, 40 (1989) 1615.
[104] R. Dickman and M.A. Burschka, Phys. Lett. A, 127 (1988) 132.
[105] R. Dickman, Phys. Rev. A, 40 (1989) 7005.
[106] T. Aukrust, D.A. Browne and I. Webman, Europhys. Lett., 10 (1989) 249.
[107] J.W. Evans and C.A. Hurst, Phys. Rev. A, 40 (1989) 3461.
[108] S. Katz, J.L. Lebowitz and H. Spohn, Phys. Rev. B, 28 (1983) 1655.

[109] U. Frisch, B. Hasslacher and Y. Pomeau, Phys. Rev. Lett., 56 (1986) 1505.
[110] R. Benzi, S. Succi and M. Vergassola, Phys. Rep., 222 (1992) 145.
[111] B. Chopard and M. Droz, J. Phys. A, 21 (1988) 205.
[112] J. Mai and W. von Niessen, Phys. Rev. A, 44 (1991) R6165.
[113] J. Mai and W. von Niessen, Chem. Phys., 165 (1992) 57.
[114] J. Mai and W. von Niessen, Chem. Phys., 165 (1992) 65.
[115] H. Burghgraef, A.P.J. Jansen and R.A. van Santen, Chem. Phys., 177 (1993) 407.
[116] M.A. van Daelen, Y.S. Li, J.M. Newsam and R.A. van Santen, J. Phys. Chem., 106 (1996) 2279.